

# Magnetic Properties of Metric Noise Storms Associated with Coronal Mass Ejections \*

Ya-Yuan Wen, Jing-Xiu Wang and Yu-Zong Zhang

National Astronomical Observatories, Chinese Academy of Sciences, Beijing 100012; [wenny@bao.ac.cn](mailto:wenny@bao.ac.cn)

Received 2006 June 16; accepted 2006 August 3

**Abstract** Using Nançay Radioheliograph (NRH) imaging observations, combined with SOHO/Michelson Doppler Imager (MDI) magnetogram observations and coronal magnetic field extrapolation, we studied the magnetic nature of metric noise storms that are associated with coronal mass ejections (CMEs). Four events are selected: the events of 2000 July 14, 2001 April 26, 2002 August 16 and 2001 March 28. The identified noise storm sources cover or partially cover the active regions (ARs), but the centers of storm sources are offset from the ARs. Using extrapolated magnetic field lines, we find that the noise storm sources trace the boundary between the open and closed field lines. We demonstrate that the disappearance of noise storm source is followed by the appearance of the burst source. The burst sources spread on the solar disk and their distributions correspond to the extent of the CME in LASCO C2 field of view. All the SOHO/Extreme Ultraviolet Imaging Telescope (EIT) dimmings associated with noise storm sources are located at the periphery of noise storms where the magnetic lines of force were previously closed and low-lying. When the closed field becomes partially or fully open, the basic configurations of noise storm sources are changed, then the noise storm sources are no longer observed. These observations provide the information that the variations of noise storms manifest the restructuring or reconfiguring of the coronal magnetic field.

**Key words:** Sun: corona — Sun: coronal mass ejection (CME) — Sun: radio radiation

## 1 INTRODUCTION

The solar noise storm discovered by Hey (1946) has been one of the longest studied phenomena by solar radio astronomers. Noise storms at decimetric and metric wavelengths consist of a continuum and superposed short-lasting (1 s), narrow-band (1 MHz) bursts. Elgarøy (1977), Benz & Zlobec (1982) and Kai et al. (1985) believed that the storm sources are located in large-scale magnetic structures above active regions (ARs), sometimes in regions interconnecting ARs, and could be maintained over timescales of hours or even days. It is now well established that the occurrence of noise storm is closely associated with the observed changes of sunspot groups in the photospheric magnetic field (McLean 1981; Brueckner 1983; Stewart et al. 1986; Bentley et al. 2000). It is recognized that the nonthermal electrons that are involved in generating the noise storm continua are probably accelerated in closed coronal loops above active regions. Noise storm continua are sometimes accompanied by coincident (thermal) soft X-ray brightenings (Raulin & Klein 1994; Krucker et al. 1995; Crosby et al. 1996), which are also signatures of coronal magnetic field evolution. However, the duration of the noise storm is much longer than the X-ray emission, and consequently continual electron acceleration is required. The acceleration is probably triggered by the same processes that give rise to the X-ray brightenings accompanying the onset of the noise storms.

---

\* Supported by the National Natural Science Foundation of China.

Many authors agree that the noise storms are due to suprathermal electrons emitting radio waves through a two steps mechanism: generation of Langmuir waves and their conversion to transversal waves by coalescence with some often unspecified low frequency waves (Benz & Wentzel 1981; Spicer et al. 1982; Melrose 1980). A general consensus exists that the radiation is emitted at or close to the local plasma frequency. Some single-event analyses show that noise storms may start in association with disappearing prominences (McLean 1973; Webb & Kundu 1978; Lantos et al. 1981; Kundu & Gopalswamy 1990) and the launch of a coronal mass ejection (CME) (Lantos et al. 1981; Lantos 1982). Raulin & Willson et al. (1991) noted that there was some similarity of the onset of the noise storm with the onset behavior of flares and CMEs (Raoult et al. 1985; Machado et al. 1988; Harrison & Sime 1989; Willson et al. 1990). Kerdraon et al. (1983) have shown that the onsets or enhancements of noise storms are systematically accompanied or preceded by the addition of material in the corona. This indicates that the local plasma magnetic field is restructuring at the time and the place where the noise storms are emitted.

Recently, CMEs have been one of the most extensively studied phenomena of coronal activity. The activities between noise storms and CMEs have become one of the interesting topics. Ramesh et al. (2001) performed a statistical study of the metric noise storm continuum sources near the solar limb and verified that changes in noise storms were often followed by a CME at the solar limb, with the noise storm contained within the angular span of that particular CME. Chertok et al. (2001a, b) have discussed a little-known variety of sharp decreases of long-duration meter-wavelength noise storms and type IV bursts by the IZMIRAN observations. It showed that the strong coronal disturbance associated with a halo CME appeared to result in noticeable restructuring of the pre-existing noise storm of metric wavelengths. The variations of the noise storm emission appeared to be one of the radio manifestations of a rising CME and its interaction with coronal structures. These studies revealed that the coronal restructuring that leads to changes in noise storm behavior would shed new light on the understanding of source regions and initiation of CMEs. This provided the motivation for an ongoing study of noise storm changes and the associated Earth directed (halo) CMEs.

In this study, we confine our attention primarily to the solar activity close to the solar center, using imaging observations from the Nançay Radioheliograph (NRH) (Kerdran & Delouis 1997), combining the photospheric magnetic field observations and coronal magnetic field extrapolation, to study the magnetic nature of the metric noise storm associated with CMEs. NRH at radio wavelengths plays a key role for studying the source region of CMEs. It can provide an important diagnostic for understanding the initiation and development of CMEs. The NRH measurements provide images of radio emissions in the frequency range 160–450 MHz, corresponding to lower coronal levels within about  $\leq 2R_{\odot}$ . The time of NRH observations usually starts at about 08:00 UT and ends at around 15:30 UT every day. We use the data from SOHO's Michelson Doppler Imager (MDI) (Scherrer et al. 1995) to extrapolate the magnetic field lines from the photosphere surface to the corona. SOHO's Extreme Ultraviolet Imaging Telescope (EIT) (Delaboudinière et al. 1995) observations are also used to discuss the relationship between the noise storm positions and the EUV dimmings.

Four events were selected from Zhou et al. (2003, 2006) list of all the sampled CMEs. They are the events of 2000 July 14, 2001 April 26, 2002 August 16 and 2001 March 28. The criterion of selection is as follows. (1) The solar surface activity is close to the disk center, usually between  $\pm 30^{\circ}$  in longitude and latitude. (2) The activity takes place during the observation period of the NRH. (3) The noise storm events can be found in Solar Geophysical Data which regularly publishes the exact location and start time of events observed with the NRH. (4) The events are of the simpler type, including one or two CMEs during the observation period of the NRH.

The next section of the paper is devoted to the data analysis. We first give a detailed analysis of the event on of 200 July 14, then a simple description of the other three events. In the NRH observation it is necessary to define the noise storm and burst in this study. The noise storm is defined when short-lasting (1 s), narrow-band (1 MHz) type I bursts are superposed on a slowly varying continuum. It could be maintained over timescales of hours or even days. Whenever there is radio emission enhancement and the radio flux begins to increase, the burst appears on the Sun's disk. It jumps in position and the duration is very short. Usually, the burst belongs to type I, II, III, IV or V. Finally in Section 3 we present a summary and a discussion.

## 2 OBSERVATION AND ANALYSIS OF THE EVENTS

### 2.1 The 2000 July 14 Event

#### 2.1.1 Observation of the NRH

The Bastille Day event of 2000 involves, besides NOAA AR9077, several smaller ARs such as AR9073, AR9081, AR9082 and so on (see Fig. 1). Most of the ARs that can be identified on the Sun on July 14 have associated weak noise storms (Maia et al. 2001; Wen et al. 2005). Before the event the filaments in AR9077 and AR9082 merged into a trans-equatorial filament from north to south (Wang et al. 2006). The filament in AR9077 could be considered as a part of a huge filament. A global eruption of the trans-equatorial filament started approximately from 08:22 UT. The filament in AR9077 began to break out at about 10:02 UT. The trans-equatorial filament completely disappeared after 10:16 UT. Prior to the onset of the X-flare in AR9077 there was a series of noise storm (their positions on the Sun are shown in Figure 2). The strongest one is associated with AR9077. One of the weaker sources, marked by white arrows, is associated with AR9073 and AR9069.

The source positions are higher in altitude at 164 MHz than at the other three frequencies, thus may suffer more severe projection effects. To match the radio sources and the magnetic flux distribution in the photosphere is a rather difficult task. The correlation of the sources with magnetic field configuration can be facilitated by allocating the projected positions of the sources along the vertical (or the local solar vector radius) direction in the magnetogram (Wen et al. 2006). However, it is not granted that the radio sources

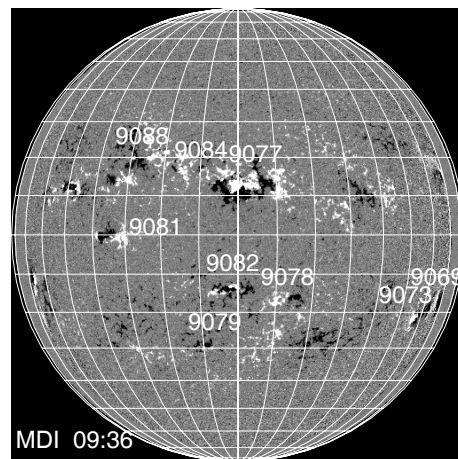


**Fig. 1** Positions of ARs on 200 July 14, 2000. An X5.7 flare occurred in AR9077 at about 10:00 UT.

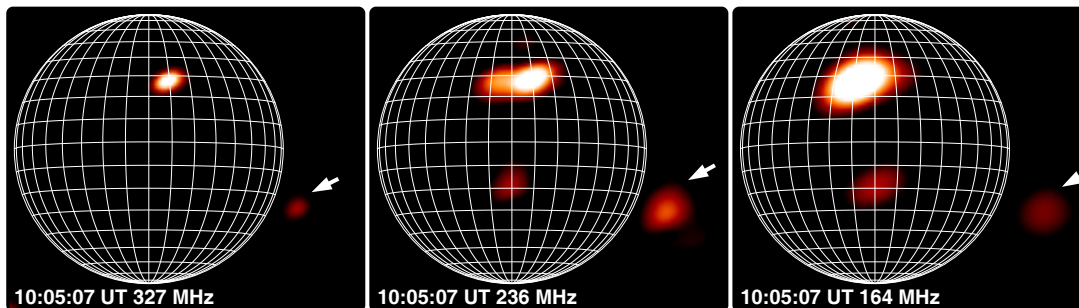


**Fig. 2** NRH images at 327, 236 and 164 MHz showing the positions of several noise storm centers on the Sun, a few minutes before the onset of the major Bastille day event.

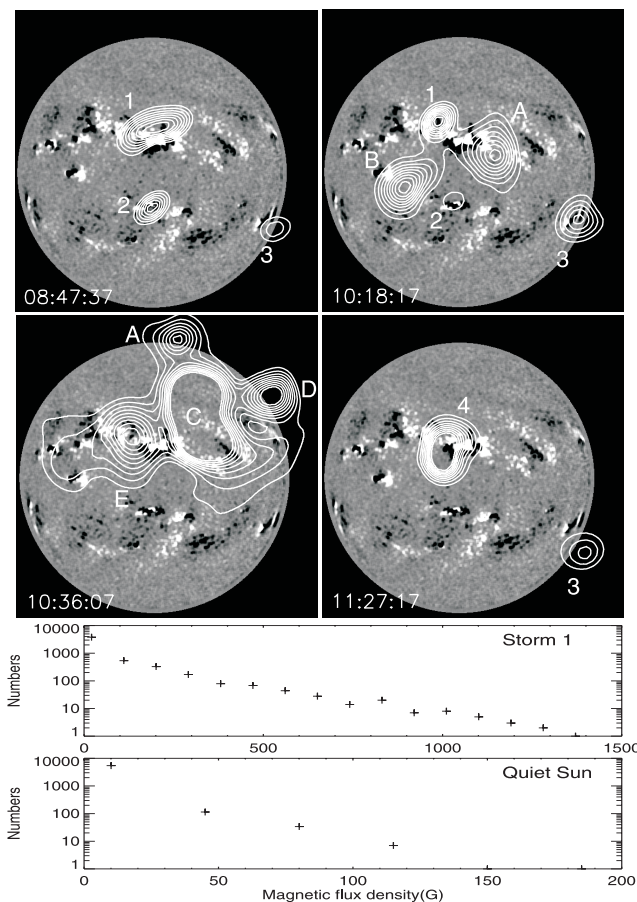


**Fig. 3** NRH projections of the storm sources and burst sources at 164 MHz on the solar surface along the solar radius are superimposed on the MDI magnetogram. The contour levels are  $0.14 \times 10^8 \sim 1.14 \times 10^8$  G. The noise storm sources are marked by numbers, while the burst sources are marked by letters (top). The plots showing the magnetic flux density distribution of storm sources and of the quiet Sun (bottom).

are necessarily connected vertically to the magnetic field in the lower atmosphere. Therefore, this does not seem to bring additional arguments on the correlations. The following discussions on the correlation of radio sources and magnetic field distribution are only referring to the gross magnetic structure and are tentative. Figure 3 shows the positions and spatial evolution of the storm continuum sources and burst sources at 164 MHz of the NRH. To show the large scale field distribution, the magnetogram has been smoothed by  $8 \times 8$  arcsec. The sources labelled by numbers (1, 2, 3, 4) are storm continuum sources, while those labelled by letters (A, B, ..., E) are burst sources. From around 08:27 UT three storm sources are becoming more stable. The south of storm source '1' covers AR9077 and AR9084, its north covers a large unipolar region, while its center is displaced from the ARs. Storm source '2' covers AR9082 and the region between AR9082 and AR9078. Storm source '3' is located outside the southwestern limb from the beginning at a height of about  $(1.38 \pm 0.33)R_{\odot}$  from the solar center and covers AR9073 and AR9069. At 10:18 UT, burst sources 'A' and 'B' were observed on the disk. The source 'B' appeared to be where the trans-equatorial filament lay. Both the storm sources and burst sources spread nearly all over the solar disk at that time and the flux intensity started to rise and the structure of the radio emission regions became increasingly complex. After 10:20 UT, the storm sources '1', '2' and '3' could no longer be detected, the discrete burst sources were moving. The burst source 'A' appeared to move in the north-west direction. At about 10:36 UT, the burst sources covered nearly all the visible range in longitude and a huge span in latitude. It indicated that the halo

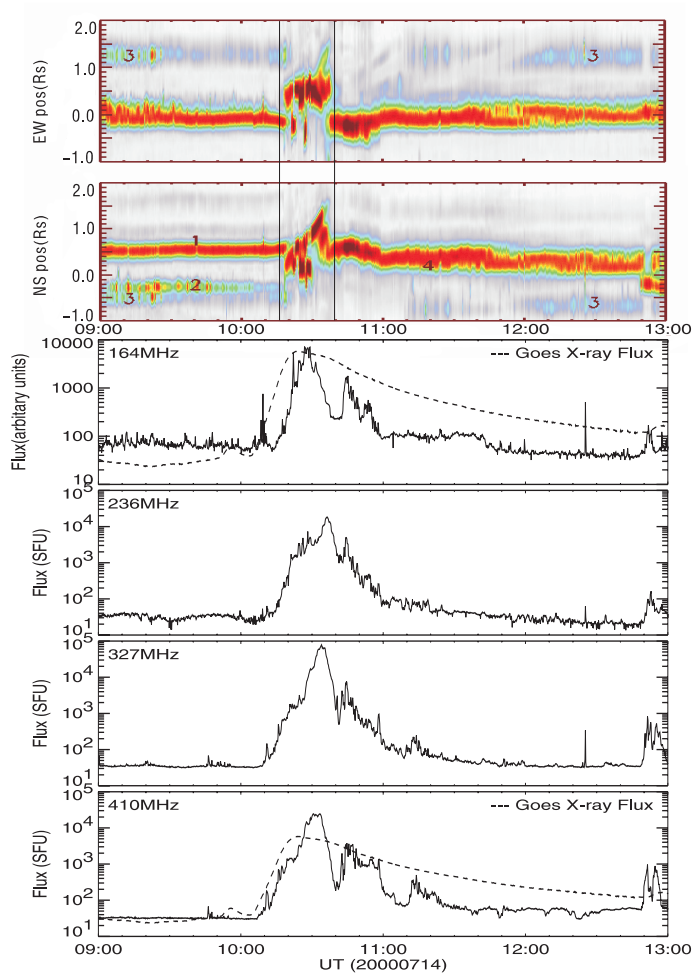


**Fig. 4** One-dimensional plot showing a series of noise storm continuum sources (labelled by numbers) and burst sources (marked by vertical lines). The vertical axis denotes the E-W position or N-S position with West or North on top. Note the changes in the flux level before and after the CME event. The GOES X-ray flux of the flare is superposed with the dashed curve (bottom).

CME was being ejected to all directions. After 11:00 UT, the storm sources ‘1’ and ‘2’ do in fact disappear, storm source ‘3’ and a new storm source ‘4’ are visible on the disk. It seems that storm source ‘4’ partially cover AR9077 and AR9084, it is to the south-east of storm source ‘1’. To identify the magnetic flux density distributions of storm sources, we compare them with that of quiet Sun, the result is shown in the bottom of Figure 3. It can be seen that the storm sources cover the regions between the ARs and the large-scale unipolar region.

Given the complexity of the radio emission, we use one-dimensional dynamical scans from the two-dimensional images to follow simultaneously the progression of the sources in intensity, position and time (Maia et al. 2004). In Figure 4, the storm source ‘1’ lies about  $0.33R_{\odot}$  to the north, storm sources ‘2’ and ‘3’ lie about  $0.17R_{\odot}$ ,  $0.67R_{\odot}$  to the south, respectively. At around 10:20 UT, the storm sources could not be observed, the burst began to get complex. After 11:00 UT, the burst became weaker, the storm sources ‘1’ and ‘2’ disappeared, a new storm continuum source ‘4’ appeared in an intermediate position, while storm source ‘3’ seemed to survive, though slightly shifted. The global flux showed apparent variations. Before 10:20 UT, the flux level at 164 MHz kept around 70 SFU, then it increased very quickly and then began to

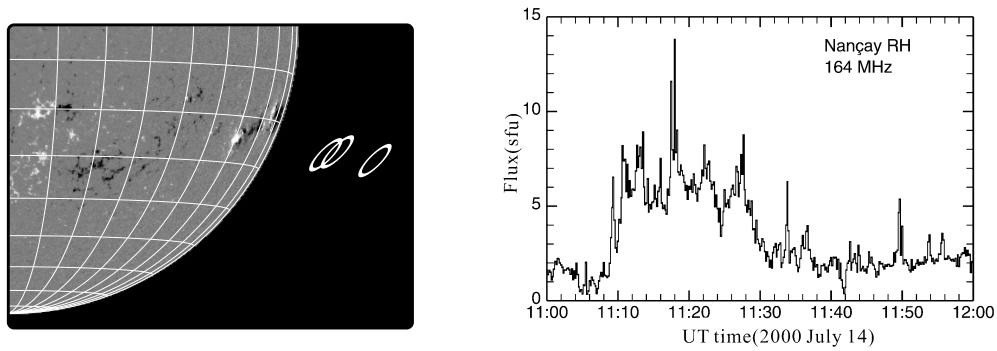


**Fig. 5** MDI magnetogram on which positions of the centers of noise storm labelled 3 on the west limb are marked. The ellipse close to the limb marks the position at 327 MHz, the ellipse in the middle marks the position at 236 MHz, and the outer one marks the position at 164 MHz (left). Flux at 164 MHz of the same noise storm center associated with the complex AR9073 and AR9069, during the period of the minor Bastille event (right).

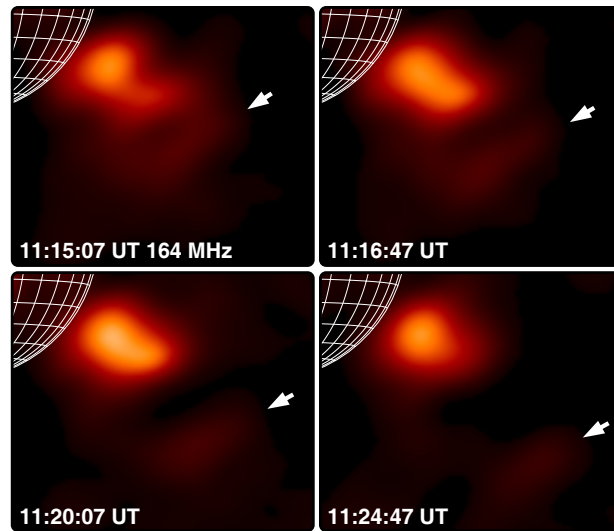


**Fig. 6** NRH images at 164 MHz showing the progression of a radio CME, whose leading edge is marked with white arrows.

drop between 10:20 UT and 11:00 UT; then at about 11:50 UT, the flux dropped substantially, apparently to lower than before 10:20 UT, indicating a weaker storm after the strong radio emission. This conclusion agrees with that of Chertok et al. (2001a). To show the weakness of the noise storm, we calculated the mean value and standard deviation of flux levels. The result is  $71 \pm 33$  SFU before 10:20 UT and  $46 \pm 28$  SFU after 11:50 UT. So it indicates that the noise storms must have undergone significant variations during the big event. Such variations of the noise storms appear to be one of the radio manifestations of a rising CME and its interaction with coronal structures (Chertok et al. 2001b). There is no obvious flux changes in other three frequencies before and after the event. It is also noticed that the X-ray enhancement accompanies the noise storm emission during the event.

Interestingly, the position of storm source ‘3’ did not change significantly in the images at 11:00 UT, after the perturbations associated with the major Bastille event have faded significantly. Because we have

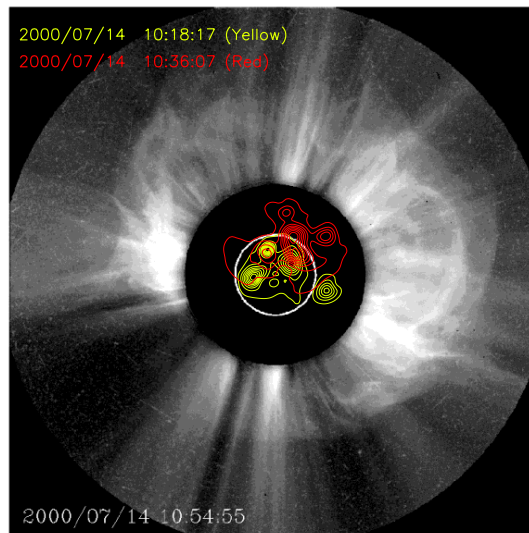


**Fig. 7** 164 MHz intensity contours of noise storm sources and burst sources along the line-of-sight around 10:18 UT (yellow) and 10:36 UT (red), observed by the NRH superimposed on the SOHO/LASCO C2 image at 10:54 UT on 2000 July 14.

access to multiple frequency data that correspond to different height ranges we can assess the projection effects. The arrangement of source positions in height is clearly seen in Figure 5 that shows the several positions of storm source ‘3’. Then, at around 11:02 UT, AR9073 and AR9069 experienced some minor sub-flare activity, peaking at around 11:04 UT and lasting until about 11:40 UT. This marks the onset of what we call ‘the minor Bastille Day event’. Associated with this flaring activity, there was a rather weak enhancement in flux level in the region of the noise storm centers above AR9073 and AR9069. The weak increase is only about 10 SFU, and can only be seen because the strong non-thermal radio activity associated with the major Bastille Day event had subsided considerably (see Fig. 5). For comparison, we note that during the major Bastille day event the flux at 164 MHz peaks at about 10000 SFU. Even during the quieter phase when the minor Bastille Day is seen, the small rise in the flux accounts for only a few percent of the total solar flux at 164 MHz. The remarkable aspect of the event is not in the minor flaring, but in what the radio images at 164 MHz reveal a radio source, whose shape in its early stages is that of a loop, moves from the noise storm region at a velocity about  $580 \text{ km s}^{-1}$  around the direction  $45^\circ$  south. The moving feature is very faint, the brightness is just barely above the instrument noise (see Fig. 6). The moving radio feature is seen up till 11:30 UT, when it fades into the background noise. This corresponds to the time when the radio flux at the noise storm positions drops also to the lower values. The link between the activity at the vicinity of the noise storm site and the moving source is thus clear.

### 2.1.2 Comparison between the Sources and the Initiation of the Halo CME

It is well known that the initiation and early development of CME are difficult to detect and estimate owing to occulting disk of the coronagraph. Imaging observations at radio wavelengths can serve as a supplement for observing the initiation and development of the CME in the low corona. The intensity contours of noise storm sources and burst sources at 10:18 UT and 10:36 UT are superimposed on the SOHO/LASCO C2 field of view image, the result is shown in Figure 7. At around 10:18 UT, the radio emission which spreads over the solar disk marked the initiation of the halo CME. This time is consistent with that obtained from the linear fit to the height-time data of a CME detected by LASCO (Brueckner et al. 1995). The distribution of the burst sources at about 10:36 UT corresponds well to the extent of the CME in the C2 image. The movements of the burst sources ‘A’, ‘D’ and ‘E’ involved in the halo CME in the interval of 10:18–10:37 UT show the signature of the CME development.

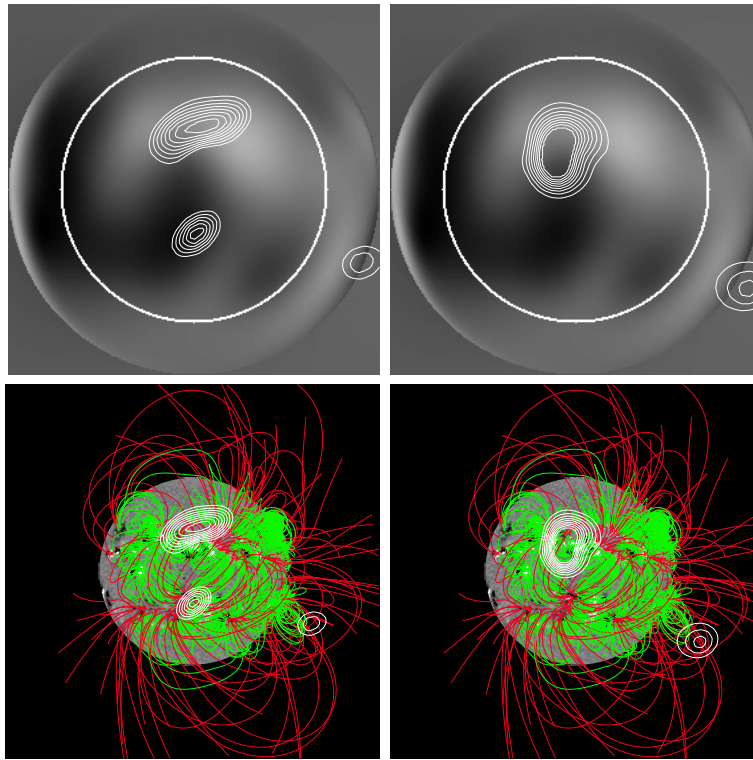


**Fig. 8** Extrapolated magnetic field distribution at  $1.4R_{\odot}$  from the solar center. The white large circle denotes the Sun disk (top). The global extrapolated magnetic field line maps calculated by the boundary element method. The noise storm sources in the line-of-sight projection at 08:47 and 11:27 UT observed by the NRH at 164 MHz are overlaid on them (bottom).

### 2.1.3 The Magnetic Connectivity of Noise Storm Sources

To identify the positions and magnetic nature of the noise storm sources, we may refer to the extrapolated coronal magnetic field from the photosphere magnetogram. This is shown in Figure 8. The top two panels are the extrapolated magnetic field distribution at  $1.4R_{\odot}$  from the solar center. The noise storm sources in the line-of-sight projection at 08:47 UT and 11:27 UT observed by the NRH at 164 MHz are superimposed on them. It is obvious that the extrapolated magnetic field distribution is weaker and smoother. The magnetic field configuration is larger than that of the photosphere surface. Noise storm sources ‘1’ and ‘4’ clearly cover the magnetic neutral lines between the ARs. In the bottom two panels, the potential field line maps calculated by the boundary element method (BEM, Wang et al. 2002) are composed of full-disk MDI data at 09:36 UT on July 14 and Daily Synoptic Chart (DSC) on MDI Day 2759. The green lines represent the closed field lines below  $0.4R_{\odot}$ , the red lines, the closed lines above  $0.4R_{\odot}$  and all the open field lines. The noise storms, observed in the radio images at 164 MHz, are superimposed on the map of the extrapolated magnetic field lines. It can be seen that the noise storm source ‘1’ is linked to the field lines located at the boundary between the open and closed magnetic field lines. The storm source ‘2’ is in the vicinity of a large-scale magnetic neutral line, and also above the boundary between the open and closed magnetic field structures. The storm sources ‘3’ and ‘4’ lie at the boundary between the open and closed magnetic field structure.

### 2.1.4 The Relationship between EUV Dimmings and Noise Storm Sources

To avoid the appearance of false darkenings or brightenings in the EIT running difference images, we use the base difference images (Chertok et al. 2005) in the study. All the disk images of the event are rotated to

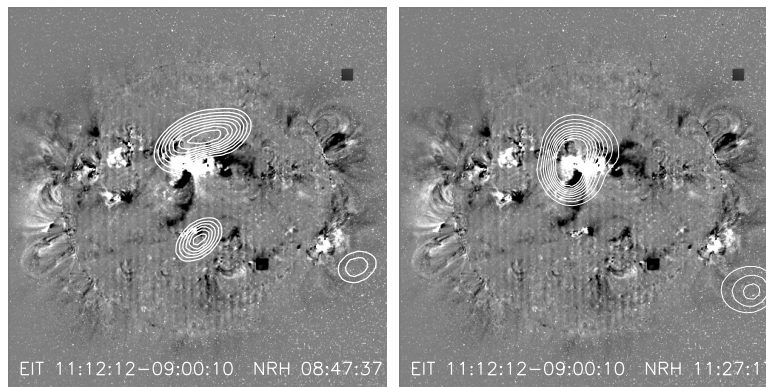


**Fig. 9** 164 MHz intensity contours of noise storm sources along the line-of-sight at around 08:47 and 11:27 UT observed by NRH, superimposed on the SOHO/EIT fixed difference image at 195Å. The two squares mark missing blocks.

a common pre-event time, then the same pre-event image is subtracted from all subsequent heliograms, and the fixed or base difference images are reconstructed. Figure 9 shows the most developed dimmings (brightness depletions) (Thompson et al. 1998; Zerro et al. 1999) for the event. There are four persistent dimming regions on the disk. The first two dimming areas extend from AR9077 toward the southern hemisphere. The third one appears in the north-west of AR9082. The fourth one is associated with AR9081, which is not associated with the noise storm sources. All the dimming regions appear to be associated with ARs. It is remarkable that all the dimmings associated with noise storm sources are located on the periphery of the noise storm where the magnetic lines of force were previously closed and lower-lying. Whenever a dimming appears during the CME onset, the noise storm sources have already disappeared. This indicates that the magnetic reconfiguration as manifested by the coronal dimming is the reason of variations in the noise storm. If we believe that the persistent dimmings seen in fixed difference images represent mass ejecta from the open magnetic field, then this adjustment would result in variations of the noise storms.

## 2.2 The 2001 April 26 Event

The event of 2001 April 26 is associated with a long filament and a GOES M7.8 flare (a 2B flare in H $\alpha$  classification), which lies in the NOAA AR9433 (N17W31). The flare began at 11:26 UT and reached its peak value at 13:12 UT. The filament erupted at 09:06 UT. The CME was first apparent at 12:30 UT in the LASCO C2 field of view.

Similar to the style of Figure 3, the positions of noise storm continua and burst sources are shown in Figure 10. From 08:19 UT, the storm continuum sources '1' and '2' are seen on the disk. They seemed to be the two components of one source. Storm source '1' covers the limb of AR9439 and a larger unipolar region. Storm source '2' covers the south-west limb of an extended bipolar region (EBR) (Zhou et al. 2006), which includes AR9433. An EBR is a type of large-scale magnetic structure which is CME-prolific. At around 11:38 UT, the radio emission began to increase. At 11:45 UT, the storm source '2' could not be observed and more burst sources were visible on the disk. It indicated that the CME was starting. At 12:40 UT the storm source '3' appeared above the EBR and covered the large-scale magnetic neutral line of the EBR. The disappearance of storm source '2' and the appearance of storm source '3' after the event indicate that these changes are evidence of restructuring or reconfiguring of the large-scale magnetic field. It also indicates that the variations of storm sources are the signature of large-scale source region of halo CME. Storm source '1' existed during the whole event, which means that the storm source '1' was not involved in the interaction of large-scale magnetic field lines. The global flux level apparently varied. At around 11:40 UT, the flux level began to rise, at about 12:00 UT it began to drop, at about 12:40 UT it rose again, but to a level lower than before 11:40 UT. The mean values and standard deviations of the flux level are  $185 \pm 34$  SFU before

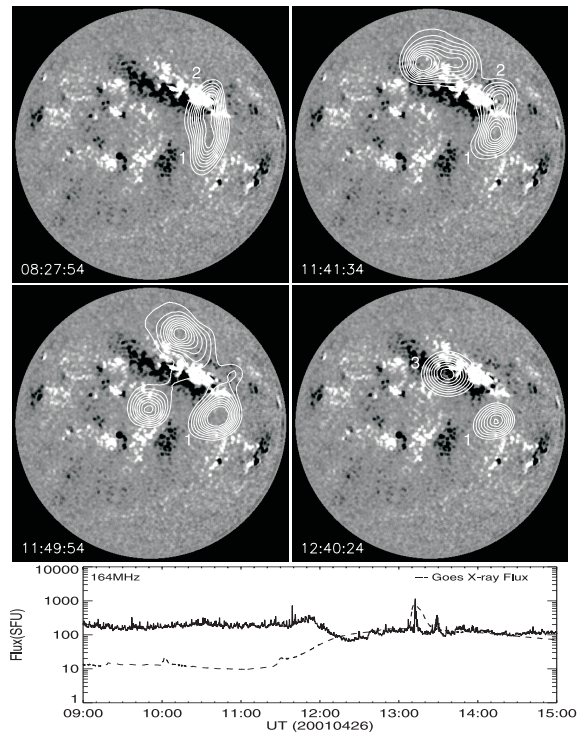


**Fig. 10** 164 MHz NRH projections of the storm sources and burst sources on the solar surface along the solar radius are overlaid on the MDI magnetogram. The contour levels are  $0.44 \times 10^8 \sim 3.08 \times 10^8$  K (top). Evolution of global flux at 164 MHz and the GOES X-ray flux of the flare (bottom).

11:40 UT and  $130 \pm 61$  SFU after 12:40 UT. It is also noticed that X-ray enhancement accompanied the noise storm emission during the event.

In the top two panels of Figure 11, the storm sources are overlaid on the extrapolated magnetic field lines. It seems that noise storm sources '1', '2' and '3' are linked to field lines located at the boundary between the open and closed magnetic field lines. In the bottom two panels, there are two large persistent dimming regions associated with the noise storms '2' and '3'. They extend from AR9433 toward the south-west. The dimmings associated with the noise storm sources are also located on the periphery of the noise storms where the magnetic lines of force were previously closed and lower-lying. This conclusion is consistent with the above event. There appears to be no connection between the dimmings and noise storm '1'. So, noise storm '1' was not involved in the restructuring of the coronal magnetic field and it underwent no changes before and after the CME event.

### 2.3 The 2002 August 16 Event

The CME observed on 2002 August 16 is associated with a GOES M5.2 flare (a 2N flare in the  $H\alpha$  classification) beginning at 11:32 UT in NOAA AR 10069 (S14E20). The halo CME was first observed at 12:30 UT in the LASCO C2 field of view.

Figure 12 shows the positions and spatial evolution of the storm continua and burst sources at 164 MHz of the NRH. The noise storm sources are labelled by numbers. From 08:25 UT, the storm source '1' covered AR10069 and its boundary. At around 11:30 UT, the radio emission began to rise. At 12:00 UT, the storm source '1' could not be seen and two burst sources were visible at the limb of the disk. It indicated that the CME had begun. At 12:05 UT, noise storm '2' was observed on the solar disk, covering ARs 10068 and 10069 and a large-scale unipolar region. The disappearance of storm source '1' and the appearance of storm source '2' after the halo CME event also indicate that the storm source changes demonstrate

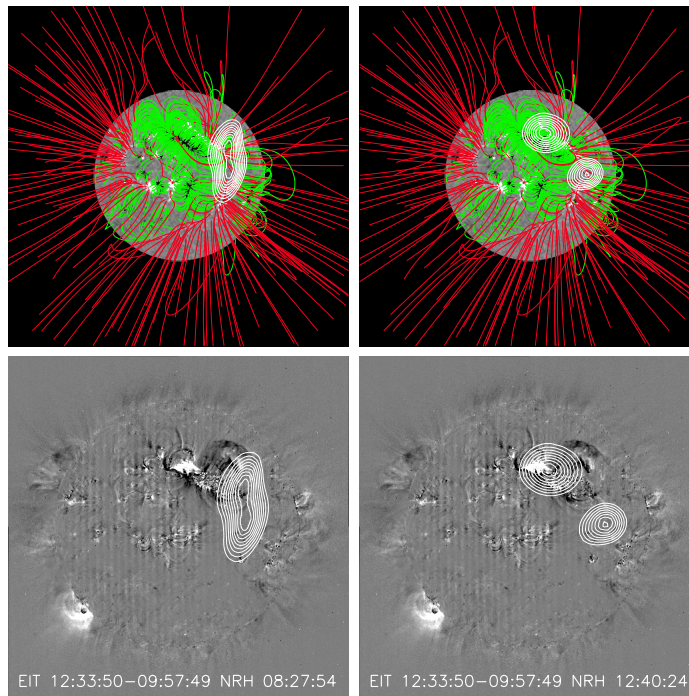


**Fig. 11** 164 MHz NRH projections of the noise storm sources along the line-of-sight at 08:27 and 12:40 UT, superimposed on the extrapolated potential field line maps (top) and SOHO/EIT fixed difference images (bottom).

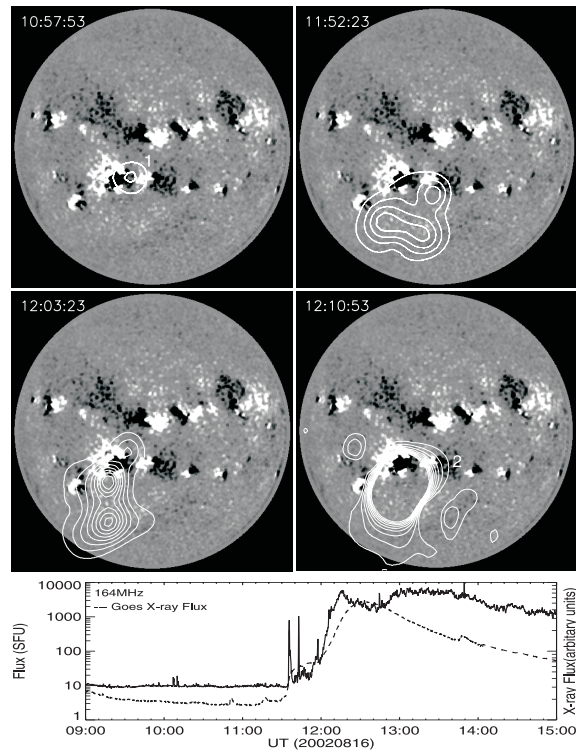
the restructuring or reconfiguring of the coronal magnetic field. The global flux level showed apparent variations. At around 11:30 UT, the flux level began to rise, at about 12:15 UT, it reached its maximum, then it began to fall slowly, but remaining much higher than before 11:30 UT. The mean values and standard deviations are  $10 \pm 0.9$  SFU before 11:30 UT and  $2931 \pm 1662$  SFU after 12:10 UT. During the event it is also noticed that X-ray enhancement accompanied the noise storm emission.

Figure 13 shows the relationship between noise storm source positions and EUV dimmings. There are two dimming regions on the south-east disk, extending from AR10069 in the south-east direction. It is noticeable that, again, the dimmings are located on the periphery of the noise storms where the magnetic lines of force were previously closed and lower-lying, — as in the two previous events.

#### 2.4 The 2001 March 28 Event

The CME of 2001 March 28 was associated with a GOES M4.3 flare (an SF flare in  $H\alpha$  classification). It was in the NOAA AR9393 (N18E02). The flare began at 11:21 UT and peaked at 12:40 UT. The halo CME was first apparent at 12:50 UT in the C2 field of view. In this event, besides NOAA AR9393, there were several smaller ARs that were related to the event, such as AR9394, AR9402, AR9400 and so on.

In Figure 14 the style is similar to above three events. The storm continuum sources are labelled by numbers, while the burst sources are marked by letters. From 08:39 UT, the northern part of noise storm '1' covered AR9393, AR9394 and a larger unipolar region. The storm source '2' covered the peripheries of AR9390, AR9400, AR9402 and a larger unipolar region. The burst source 'A' was seen on the east of storm source '1' between 12:10 and 12:20 UT, indicating the initiation of the CME. At 12:30 UT, the storm source '2' could no longer be observed on the disk. The disappearance of storm source '2' after the halo CME event indicates that such variation in storm sources is again evidence of restructuring or reconfiguring of the coronal magnetic field. The global flux began to increase at about 09:45 UT, reached the maximum at 12:10 UT, then began to fall. After 12:30 UT, the flux began to rise again. At around 12:45 UT, the flux



**Fig. 12** 164 MHz NRH projections of the storm sources and burst sources on the solar surface and along the solar radius, superimposed on the MDI magnetogram. The contour levels are  $0.01 \times 10^8 \sim 8.01 \times 10^8$  K (top). The global flux at 164 MHz shows variations before and after the CME event. The dashed curve is the GOES X-ray flux of the flare (bottom).

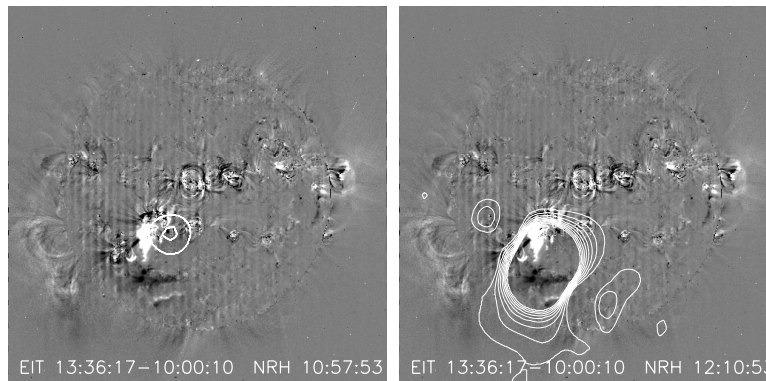


**Fig. 13** 164 MHz NRH noise storm sources projected on the line-of-sight at 10:57 and 12:10 UT are overlaid on the EIT fixed difference images.

fell until 13:10 UT. There was no obvious variation before 12:10 UT and after 13:10 UT. The intensity of the storm source '1' is higher than that of the storm source '2', so the disappearance of the storm source '2' did not significantly effect the global flux level. It is also noticed that the X-ray enhancement accompanied the noise storm emission during the event.

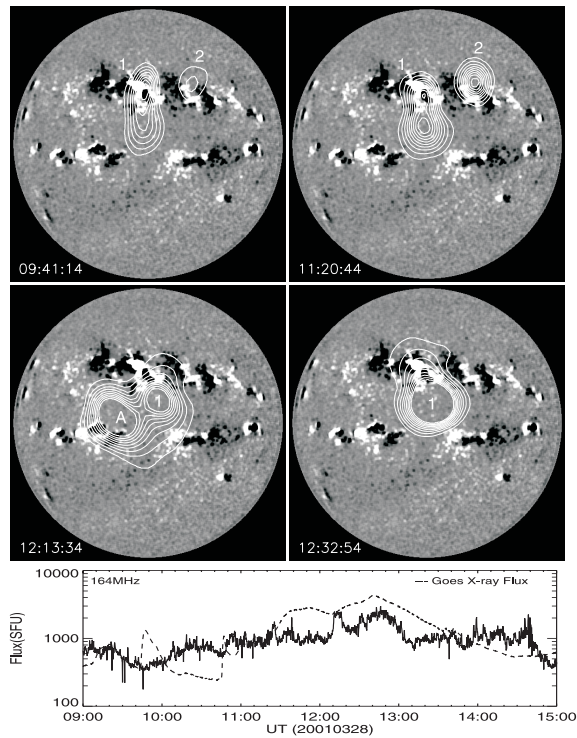


**Fig. 14** 164 MHz NRH projections of the storm sources and burst sources on the solar surface and along the solar radius, overlaid on the MDI magnetogram. The contour levels are  $0.95 \times 10^8 \sim 21.5 \times 10^8$  K (top). GOES X-ray flux of the flare overlaid on the global flux at 164 MHz (bottom).

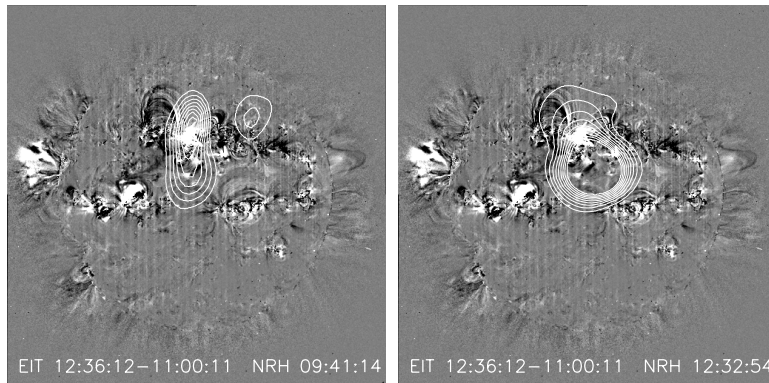


**Fig. 15** 164 MHz NRH noise storm sources projected along the line-of-sight, overlaid on the EIT fixed difference at  $195\text{\AA}$ .

The relationship between noise storm source positions and EUV dimmings is shown in Figure 15. There were mainly three dimming regions on the disk. Two were associated with the noise storm '1' that extended from the ARs to the east. They are located on the periphery of noise storm '1' where the magnetic lines were previously closed and lower-lying. Another dimming associated with noise storm '2' extended from the ARs southward.

### 3 SUMMARY AND DISCUSSION

In this study, we presented four observational events close to the center of the solar disk to show the location and evolution of the noise storm continuum sources before and after the CME event by the NRH observations. All four events belong to one category: the pre-event noise storm disappears after the CME event, and sometimes a new noise storm is observed at another position. A few properties common to these four events can be summarized as follows.

First, the noise storms are more stable before the CME event. The noise storm sources cover or partially cover the active regions, but the centers of storm sources are offset from the ARs. When the radio emission and the global flux begin to increase, the noise storm sources can not be observed and the burst sources are visible on the solar disk. Moreover, the distributions of burst sources correspond well to the extent of the CME in the C2 images. This indicates that the CME has begun to eject. After the CME event, some pre-event storm sources disappear, while sometimes new storm sources appear in other positions.

Secondly, regarding the variation of the global flux, the flux level before the CME event is usually not the same as after the event: in two of the four events, there was a sharp decrease, in a third, an obvious increase, while in the fourth, there was no obvious change. We speculate that the flux change depends mainly on the magnetic property of the noise storms. We also confirm that the X-ray enhancement accompanies the noise storm emission during the event.

Thirdly, we reconstruct the coronal magnetic field line map by extrapolation from the photosphere surface, then project on to it the noise storm sources in the line-of-sight direction. We find that noise storm sources trace the boundary between the open and closed field lines.

Fourthly, the relationship between noise storm positions and the EUV dimmings also shows that the noise storm changes signal restructuring or reconfiguring of the coronal magnetic field. It has been demonstrated that the dimming represents the opening of previously closed magnetic structures and outflow of magnetized plasma (Chen et al. 2002; Harra & Sterling 2001, 2003). It is remarkable that all the dimmings associated with noise storm sources are located at the periphery of noise storms where the magnetic lines of force were previously closed and low-lying. If we believe that persistent dimmings seen in fixed difference images represent the mass ejecta from the open magnetic lines of force after the halo CME, it may indicate that storm sources take place in the conjunction of multiple closed magnetic field structures. Whenever the closed field became partially or full opened, the basic configuration of storm sources was changed, then the storm sources were no longer observed.

The above observational facts, disappearance of pre-event noise storms after the flare/CME event, eruptions and shifting of burst sources at different parts of the disk at the low corona, evolution of CME, and appearance of the new noise storms, indicate a process involving conversion of stored magnetic energy into kinetic energy, which would also contribute to the propagation of the CME disturbance into the interplanetary medium. The strong coronal disturbance associated with the halo CME appeared to result in the noticeable restructuring of the pre-existing noise storm at metric wavelengths. It has long been known that noise storms prefer to occur above complex active regions containing emerging and decaying magnetic fields (Elgarøy 1977; Willson 2005). So the origin of noise storms is magnetic. Especially, in the event of 2001 April 26, the noise storm lies above an EBR, which is a type of large-scale magnetic structure. This implies again that CMEs are hosted by large-scale magnetic structure. It may be involved in large or even global magnetic interaction and large-scale coronal field restructuring.

As an added bonus we were able to detect a radio CME, associated with a flux enhancement in a noise storm center very far from the active center at the origin of the X-flare on 2000 July 14. Radio CMEs (Bastian et al. 2001) are interpreted as being due to synchrotron emission from electrons with energies around 1 MeV. The minor Bastille event showed there was a CME launched about an hour later from the halo associated with the major event. The CME associated with the minor event was closer to the west limb, at about 45 degrees south. This event can not be detected in LASCO coronagraphic images due to the high levels of “snow” arising from the energetic particles hitting the CCD. Accompanying the launch of this CME was a source of high-energy particles, which are what allow for the CME to be seen in radio images. This CME and source of particles clearly need to be taken into consideration in studies involving Ulysses data, since on 2000 July 14 those experiments have been magnetically connected to the west limb at a latitude of 55 degrees south.

**Table 1** Nature of Noise Storm and Associated Solar Activity

Data	Noise Storm				Flare			CME UT
	Position	Start UT	End UT	Flux (SFU)	Class	Position	NOAA	
2000-07-14	W0.06N0.33	08:27	10:20	20~100	X5.7	N22W07	9077	10:54
	W0.17S0.17	08:27	10:20	20~100				
	E0.09N0.25	11:00	15:27	20~100				
	W1.15S0.67	08:27	15:27	5~20				
2001-04-26	W0.64N0.06	08:19	15:18	20~100	M7.8	N17W31	9433	12:30
	W0.73N0.48	08:19	11:45	20~100				
	W0.22N0.36	12:39	15:18	100~300				
2002-08-16	E0.19S0.31	08:25	12:00	5~20	M5.2	S14E20	10069	12:30
	E0.39S0.56	12:05	15:25	> 300				
2001-03-28	W0.11N0.19	08:39	15:26	>300	M4.3	N18E02	9393	12:50
	W0.28N0.67	08:39	12:30					
Remark	The noise storm sources cover or partially cover the active regions, but the centers of storm sources offset to ARs. Seen from the extrapolated magnetic field lines, the noise storm sources trace the boundary between the open and closed field lines. The dimmings associated with noise storm sources are located at the periphery of noise storms where the magnetic lines of force were previously closed and low-lying.							
2000-09-12	W0.16S0.3	11:50	15:17	20~100	M1.0	S17W09		11:54
2001-02-15	W0.12N0.47	13:52	15:35	<5	B8.8	N08E10		13:54
	W1.19S0.31	13:40	15:35	< 5				
2001-09-29	W0.28N0.02	12:00	15:11	<5	M1.8	N13E03	9636	11:54
	W0.85S0.64	12:30	15:11	<5				
1999-06-24	E0.43N0.20	08:23	15:23	20~100	C4.1	N29W13	8595	13:31

On the other hand, we find another three events which belong to the other category, the noise storms do not exist before the event, but they could be found after the restructuring or reconfiguring of magnetic field. This also indicates that the noise storm changes signal restructuring or reconfiguring of the magnetic field. Furthermore, there is an event, 1999 June 24 (Wen et al. 2006), belonging to a third category. An intense radio noise storm on the east hemisphere is detected at all four frequencies of the NRH before and after the CME event. It seems that this noise storm did not involve interaction of large-scale magnetic field lines. This event is similar to the noise storm '1' of 2001 April 26 and the noise storm '1' of 2001 March 28. All the events and associated natures are list in Table 1.

In conclusion, we emphasize that the noise storm sources cover or partially cover the active regions, but the centers of storm sources are offset to the ARs. The noise storm sources trace the boundary between the open and closed field lines. The dimmings associated with noise storm sources are located at the periphery of noise storms where the magnetic lines of force were previously closed and low-lying. The energy of noise storm may come from interaction and magnetic reconnection between multiple magnetic loop systems. CME is a type of adjusting and restructuring of coronal magnetic field. Variations of noise storm sources manifest this restructuring or reconfiguring. The study of the noise storm may shed new light on the understanding of the source region and the initiation of CMEs.

**Acknowledgements** We thank the Nançay Radioheliograph team for providing their image data. We also thank the SOHO/MDI and SOHO/EIT team members for providing images in the study. We are indebted to MSSL for giving us the facilities to access the various data. We are thankful to Dr. Grechnev for providing processing method of full-disk EIT images. We are very grateful to Dr. Klein and Dr. Maia for discussing the problems of noise storm. This work is supported by National Natural Science Foundation of China (Grants 10233050, 40674081 and 10573025) and the National Basic Research Program of China (2006CB806300).

## References

- Bastian T. S., Pick M., Kerdraon A., Maia D., Vourlidas A., 2001, *ApJ*, 558, L65
- Bentley R. D., Klein K.-L., Van Driel-Gesztelyi L. et al., 2000, *Solar Phys.*, 193, 227
- Benz A. O., Wentzel D. G., 1981, *A&A*, 94, 100
- Benz A. O., Zlobec P., 1982, Proc.4<sup>th</sup> CESRA workshop on Solar Noise Storms, Trieste Observatory Publication.
- Brueckner G. E., 1983, *Solar Phys.*, 85, 243
- Brueckner G. E. et al., 1995, *Solar Phys.*, 162, 357
- Chen P. F., Wu S. T., Shibata K., Fang C., 2002, *ApJ*, 572, L99
- Chertok I. M., Kahler S., Aurass H., Gnezdilov A. A., 2001a, *Solar Phys.*, 202, 337
- Chertok I. M., Fomichev V. V., Gnezdilov A. A. et al., 2001b, *Solar Phys.*, 204, 139
- Chertok I. M., Grechnev V. V., 2005, *Solar Phys.*, 229, 95
- Crosby N., Vilmer N., Lund N., Klein K.-L., Sunyaev R., 1996, *Solar Phys.*, 167, 333
- Delaboudinière J.-P., Artzner G. E., Brunaud D. et al., 1995, *Solar Phys.*, 162, 291
- Elgarøy Ø., 1977, *Solar Noise Storms*, Oxford: Pergamon Press
- Harra L. K., Sterling A. C., 2001, *ApJ*, 561, L215
- Harra L. K., Sterling A. C., 2003, *ApJ*, 587, 429
- Harrison R. A., Sime D. G., 1989, *J. Geophys. Res.*, 94, 2333
- Hey J. S., 1946, *Nature*, 157, 47
- Kai K., Melrose D. B., Suzuki S., 1985, in: D. J. McLean and M. R. Labrum (eds.) *Solar Radio Physics*, Cambridge University Press, Cambridge, Chap. 16, p.414
- Kerdran A., Delouis J.-M., 1997, in: *Coronal Physics from Radio and Space Observations*, ed. G. Trottet, Berlin: Springer, 483, 192
- Kerdran A., Pick M., Trottet G., Sawyer C., Illing R., Wagner W., House L., 1983, *ApJ*, 265, L19
- Krucker S., Benz A. O., Aschwanden M. J., Bastian T. S., 1995, *Solar Phys.*, 160, 151
- Kundu M. R., Gopalswamy N., 1990, *Solar Phys.*, 129, 133
- Lantos P., Kerdran A., Rapley G. G., Bentley R. D., 1981, *A&A*, 101, 33
- Lantos P., 1982, in: Benz A. O., Zlobec P., eds. Proc.4<sup>th</sup> CESRA workshop on Solar Noise Storms, Trieste Observatory Publication, p.247
- Machado M. E., Moore R. L., Hernandez A. M. et al., 1988, *ApJ*, 326, 425
- Maia D., Pick M., Hawkins III S. E. et al., 2001, *Solar Phys.*, 204, 199
- Maia D., Pick M., 2004, *ApJ*, 609, 1082
- McLean D. J., 1973, *Proc. Astron. Soc. Aust.*, 2, 222
- McLean D. J., 1981, *Proc. Astron. Soc. Aust.*, 4, 132
- Melrose D. B., 1980, *Solar Phys.*, 67, 357
- Ramesh R., Sundaram G. A. S., 2001, *Solar Phys.*, 202, 355
- Raoult A., Pick M., Dennis B. R., Kane S. R., 1985, *ApJ*, 299, 1027
- Raulin J. P., Kerdran A., Klein K.-L., Trottet G., Willson R. F., Lang K. R., 1991, *A&A*, 251, 298
- Raulin J. P., Klein K. L., 1994, *A&A*, 281, 536
- Scherrer P. H., Bogart R. S., Bush R. I. et al., 1995, *Solar Phys.*, 162, 129
- Spicer D. S., Benz A. O., Huba J. D., 1982, *A&A*, 105, 221
- Stewart R. T., Brueckner G. E., Dere K. P., 1986, *Solar Phys.*, 106, 107
- Thompson B. J., Plunkett S. P., Gurman J. B. et al., 1998, *Geophys. Res. Lett.*, 25, 2465
- Wang J. X., Zhou G. P., Wen Y. Y. et al., 2006, *Chin. J. Astron. Astrophys. (ChJAA)*, 6, 247
- Wang T. J., Yan Y. H., Wang J. L., Kurokawa H., Shibata, K., 2002, *ApJ*, 572, 580
- Webb D. F., Kundu M. R., 1978, *Solar Phys.*, 57, 155
- Wen Y. Y., Wang J. X., 2005, in: Dere K., Wang J. X., Yan Y. Y., eds., *Coronal and Stellar Mass Ejections*, Proc. IAU symp., 226, Cambridge Univ. Press, 141
- Wen Y. Y., Wang J. X., Maia D. et al., 2006, *Solar Phys.*, 239, 257
- Willson R. F., Lang K. R., Klein K.-L., Kerdran A., Trottet G., 1990, *ApJ*, 357, 662
- Willson R. F., 2005, *Solar Phys.*, 227, 311
- Zarro D. M., Sterling A. C., Thompson B. J., Hudson H. S., Nitta N., 1999, *ApJ*, L139
- Zhou G. P., Wang J. X., Cao Z. L., 2003, *A&A*, 397, 1057
- Zhou G. P., Wang J. X., Zhang J., 2006, *A&A*, 445, 1133